ELSEVIER

Deep-Sea Research II 52 (2005) 5–28

DEEP-SEA RESEARCH
PART II

www.elsevier.com/locate/dsr2

Mesoscale structure and its seasonal evolution in the northern California Current System

John A. Barth*, Stephen D. Pierce, Timothy J. Cowles

College of Oceanic and Atmospheric Sciences, Oregon State University, 104 COAS Admin Bldg, Corvallis, OR 97331-5503, USA

Accepted 20 September 2004
Available online 22 January 2005

Abstract

During spring and summer 2000, two mesoscale mapping cruises were carried out in the northern California Current System between 41.9°N and 44.6°N and between the shallow, inner continental shelf and up to 150 km offshore. Measurements were made using a towed undulating vehicle equipped with a conductivity-temperature-depth instrument and a chlorophyll fluorometer. A shipboard acoustic Doppler current profiler (ADCP) measured water velocities, and surface drifter trajectories and satellite sea-surface temperature imagery provide context for the mesoscale maps. Nearly identical upwelling favorable wind stresses of up to 0.2 N m^{-2} existed during both the spring and summer surveys. Early in the season (late May, early June) the upwelling front and jet followed the continental shelf bottom topography. There was cold water inshore of the shelfbreak all along the coast with pockets of elevated phytoplankton biomass (chlorophyll (chl) up to 4 mg m^{-3}) near the coast. Mesoscale activity was minimal. During late-summer (August), the upwelling front and jet were much more convoluted, including significant meanders offshore associated with a major submarine bank (Heceta Bank, 44.0–44.6°N) and a large coastal promontory (Cape Blanco, 42.8°N). High levels of phytoplankton biomass were found over Heceta Bank (chl $\sim$ 20 mg m^{-3}) and near the coast south of Cape Blanco (chl $\sim$ 10 mg m^{-3}). Low velocities inshore of Heceta Bank, measured by both shipboard ADCP and surface drifters, indicate the potential for retention of water over the Bank, leading to favorable conditions for phytoplankton biomass accumulation. The large offshore meander near Cape Blanco carried cold, nutrient-rich, high phytoplankton biomass (chl of 2–5 mg m^{-3}) water over 100 km offshore. This flow–topography interaction feature was generated in mid-June and remained an important part of the regional circulation for about 2.5 months.

1. Introduction

The northern California Current System (CCS) is the region south of the split of the North Pacific Current (West Wind Drift) offshore of the Strait of Juan de Fuca (48.5°N) and north of Cape Mendocino (40.5° N). In this region the coastline runs roughly north–south with the exception of Cape Blanco (42.8° N), which extends offshore to establish the westernmost point in the contiguous United States. The continental shelf is relatively

*Corresponding author. Tel.: +1 541 737 1607; fax: +1 541 737 2064.
E-mail address: barth@coas.oregonstate.edu (J.A. Barth).

0967-0645/$ - see front matter © 2004 Elsevier Ltd. All rights reserved.
doi:10.1016/j.dsr2.2004.09.026

narrow in the northern CCS (25–30 km) and the shelf and slope isobaths generally follow the coastline except in a number of submarine canyons off Washington and over the Heceta Bank complex (43.8–44.6°N) off central Oregon. Both Cape Blanco and Heceta Bank are known to influence the circulation in the northern CCS (Barth et al., 2000a, b; Castelao and Barth, 2005). The region is also influenced by significant freshwater input by the Columbia River (46°N) and from the Strait of Juan de Fuca (Huyer, 1983). Lastly, summertime southward, i.e. upwelling favorable, wind forcing in the northern CCS strengthens from north to south because the isobars of the North Pacific High turn from a northwest–southeast orientation off Washington and central Oregon to a north–south alignment off northern California (Huyer, 1983). At the same time, the distance between isobars decreases from north to south, and the attendant geostrophic northerly winds become stronger. While remote sensing has provided information on the circulation in this region (e.g., Strub and James, 2000), there have not been mesoscale resolving, in situ, large-area surveys of the circulation and hydrographic structure in this region like those conducted farther south (e.g., Huyer et al., 1998; Lynn and Simpson, 1987). The goal of this investigation is to describe the mesoscale structure and its seasonal evolution in the northern CCS using large-area, quasi-synoptic hydrographic, velocity and chlorophyll observations.

The Global Ocean Ecosystems Dynamics (GLOBEC) program's overall goal is to understand the effects of climate variability on the structure and dynamics of marine ecosystems and on fishery production (Fogarty and Powell, 2002). The long-term objective is to embody this understanding in ecosystem models capable of diagnosing and eventually predicting how those populations respond to environmental variability. The northern CCS was chosen as a GLOBEC study region because of its strong summertime wind-forced upwelling, by the existence of significant interannual variability (e.g., El Niño/La Niña) and because of the existence of the target species of zooplankton, salmon and their predators (Batchelder et al., 2002). Specific hypotheses of the GLOBEC Northeast Pacific (NEP) program are: spatial and temporal variability in mesoscale circulation constitutes the dominant physical forcing on zooplankton biomass, reproduction, distribution, species interactions, retention and loss in coastal regions; ocean survival of salmon is primarily determined by survival of the juveniles in coastal regions, and is affected by interannual and interdecadal changes in physical forcing and by changes in ecosystem food web dynamics.

In an effort to address these hypotheses, a large-area, mesoscale resolving sampling program was designed for the region between Newport, Oregon (44.6°N) and Crescent City, California (41.9°N), encompassing the two major topographic features Heceta Bank and Cape Blanco (Fig. 1). The sampling was conducted early in the 2000 upwelling season and again late in the summer. To investigate interannual variability (not reported here) the mesoscale surveys were repeated in 2002.

In addition to the hydrographic, velocity and chlorophyll results presented here, a 4-frequency bioacoustics instrument was towed at the surface to investigate the distributions of acoustic targets in a size range spanning copepod zooplankton to small larval fish (Ressler et al., 2005; Pierce et al., 2003; Sutor et al., 2005). An optical plankton counter mounted onboard the towed, undulating vehicle SeaSoar was used to investigate the distributions of particles, presumably zooplankton, with respect to the physical and chlorophyll fields (Zhou and Zhu, 2002). The impact of the mesoscale hydrographic, velocity and chlorophyll distributions on higher trophic levels was investigated through coordinated, concurrent sampling: surface neuston (Reese et al., 2005); gelatinous zooplankton (Suchman and Brodeur, 2005); juvenile salmonids (Brodeur et al., 2004); seabirds (Ainley et al., 2005); and cetaceans (Tynan et al., 2005).

2. Data and analysis methods

Two mesoscale mapping surveys were carried out from the R.V. *Wecoma* during 2000. The first, 29 May–17 June, was intended to sample conditions early in the upwelling season, while the

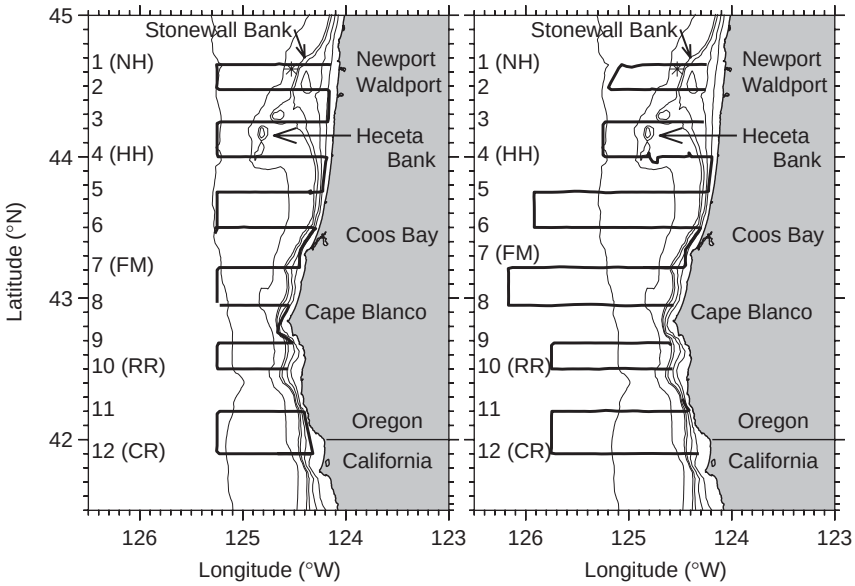

Fig. 1. Map of the GLOBEC Northeast Pacific study region with cruise tracks superimposed for the May–June (left) and July–August (right) 2000 mesoscale surveys. Line numbers are shown at left. The location of NOAA NDBC buoy 46050 off Newport is indicated by an asterisk. The 50, 70, 90, 100, 200 and 2000-m isobaths are shown.

second, 29 July–17 August, was targeted to sample fully developed summertime upwelling. The towed vehicle and shipboard ADCP sampling from the R.V. *Wecoma* was done in coordination with zooplankton sampling and bird and mammal observations from the R.V. *New Horizon*. Trawling for juvenile fish and neuston sampling were done from the F.V. *Sea Eagle*. Near real-time results from the Wecoma-based sampling were used to target some of the sampling effort by the other two vessels. The objective during each cruise was to conduct a survey of the complete study region at the start of the cruise, followed by a number of higher spatial-resolution studies of mesoscale phenomena in both the north (Heceta Bank) and south (Cape Blanco) (Fig. 1). Maps and vertical sections from the high-resolution surveys are available in O'Malley et al. (2002); however, results from those efforts are not reported here. If time permitted, a second large-scale mesoscale survey was made at the end of each cruise.

The large-scale mesoscale survey E–W sampling lines were separated by an average of 28 km (range of 19.6–33.3 km) in the N–S direction, and the entire survey took 4.5–5.4 days to complete. Several of the mesoscale survey lines (NH, HH, FM, RR and CR) were chosen to line up with transects occupied five times per year by the GLOBEC NEP Long-Term Observation Program (LTOP) cruises (Huyer et al., 2002). The large-scale mesoscale survey extended farther west in July–August to encompass the larger region of mesoscale activity during that time (see next section). Lines over the Heceta-Stonewall Bank region were chosen to avoid passing over the shallow peaks of those submarine features.

The average 28 km between-track spacing during the large-scale surveys was chosen as a compromise between a desire for coherent sampling in the alongshore direction and the goal to complete the large-scale map in approximately five days. The former is justified for physical variables (temperature, salinity, velocity) by previous studies in this region, e.g., 80(35) km alongshore correlation length scales for alongshore (cross-shelf) velocity over the mid-shelf (Kundu and Allen, 1976). In addition, the internal Rossby radius of deformation (L_R), i.e. the fundamental scale on which buoyancy and Coriolis forces balance in mesoscale structures, is 21 km in the deep-water

portion of this region (Chelton et al., 1998). Meanders and eddies arising from baroclinic instability have wavelengths of $2\pi L_R$ and diameters of πL_R, respectively, thus resolvable by the between-track spacing. Much less is known about correlation length scales of biological variables in this region, but they are likely to be anisotropic following the physical variables, i.e. shorter in the cross-front direction so resolved by the few-km SeaSoar sampling and longer in the alongfront direction. Wind and water velocity spectra from moorings in this region show a majority of energy in the "wind band" (2–10 d) over the shelf in this region Increasing to 25–150 d offshore (4200 m of water) (Huyer, 1990), hence the 5-d map duration choice.

2.1. Winds

Winds were measured at the NOAA National Data Buoy Center buoy 46050 located at 44.62°N, 124.53°W, approximately 37 km offshore of Newport, Oregon (Fig. 2). Wind stress was calculated following the method of Large and Pond (1981) and then low-pass filtered using a filter with a 40-h width at half amplitude to remove short-period (e.g., diurnal) fluctuations. To assess the cumulative alongshore wind stress during the upwelling season, north–south stress was summed starting from the spring transition defined as when winds turn to predominantly upwelling favorable (southward) usually during March to April (Huyer et al., 1979). Gaps in the NOAA NDBC buoy 46050 record were filled through regression with the nearby NOAA CMAN station at Newport, Oregon (44.61°N, 124.07°W). On the rare occasion when NDBC buoy 46050 and the Newport CMAN station were both inactive, gaps were filled through regression with the Cape Arago CMAN station (43.34°N, 124.38°W).

2.2. SeaSoar hydrography and chlorophyll

From 29 May to 17 June (Mesoscale 1) and from 29 July to 17 August (Mesoscale 2), 2000, hydrographic and bio-optical measurements were made from the towed undulating vehicle SeaSoar (Pollard, 1986). For most of the study, SeaSoar was towed using a bare hydrographic cable and profiled from the sea surface to 115–120 m over deep water and to within 10 m of the bottom over the shelf. Cycle time in deep water was about 6.5 min, resulting in surface points being separated by 1.3 km at the ship's typical 7 knot ($3.6\,m\,s^{-1}$) tow speed. Horizontal separation between profiles at mid-depth is half this value. Cycles over the shallow shelf, 0–50–0 m, took 1.5 min, so surface points were separated by about 300 m. Bottom avoidance was accomplished by using R.V. *Wecoma's* 3.5-kHz Knudsen echosounder as input to the SeaSoar flight control software.

The SeaSoar was equipped with a Seabird 911+ conductivity-temperature-depth (CTD) instrument with pumped, dual temperature-conductivity (T/C) sensors pointing forward through the nose of SeaSoar. Details of how the CTD data are processed can be found in Barth et al. (2000a). On top of SeaSoar were two Western Environmental Technology Laboratories (WET Labs) FlashPak fluorometers (WET Labs, Inc., 1997), which sampled water pumped from an intake adjacent to the T/C sensors in the nose of SeaSoar. Both fluorometers were set up to measure chlorophyll fluorescence at 685 nm, but one FlashPak used blue excitation (440 nm, 30 nm bandpass) while the other FlashPak used green excitation (490 nm, 30 nm bandpass). In this paper, we report the chlorophyll content estimated from the fluorescence measured by the "green" FlashPak. Chlorophyll fluorescence obtained by the FlashPak was calibrated against extracted chlorophyll pigments obtained from discrete samples and measured with high-performance liquid chromatography. For making horizontal maps and vertical sections, the measurements were first averaged vertically to 2-dbar bins and horizontally to 1.25 km. The usual caveats about aliasing of large-scale, low-frequency hydrographic measurements by internal waves and internal tides apply, although strong coherence in the features described here suggests that these effects are small. A complete set of the SeaSoar maps and vertical sections of all parameters can be found in O'Malley et al. (2002).

The spatially averaged temperature, salinity and pressure data are used to compute geopotential

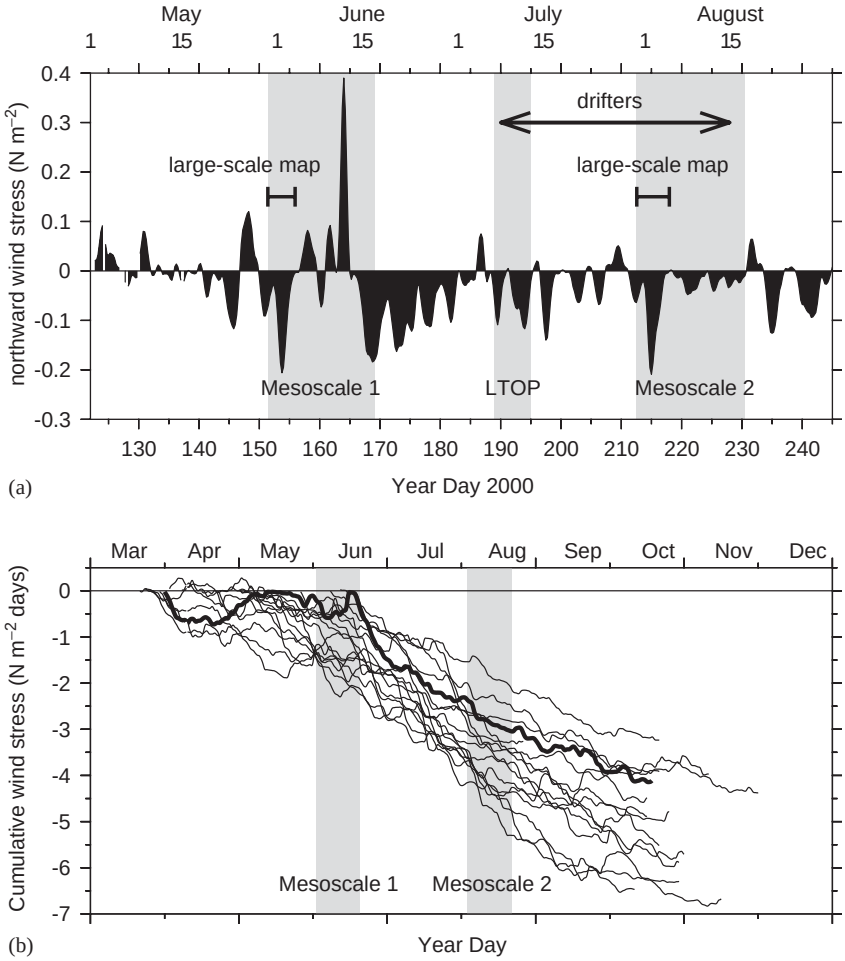

Fig. 2. (a) Wind stress from NOAA NDBC Buoy 46050 offshore of Newport, OR. (b) Cumulative alongshore (north–south) wind stress at buoy 46050 starting from the spring transition for years 1985–2000. Thick curve is cumulative stress for 2000. Gray bars indicate times of ship surveys.

anomaly (dynamic height in meters multiplied by the acceleration of gravity) in $J\,kg^{-1}$ ($m^2\,s^{-2}$) relative to 100 db. On E-W sections where the SeaSoar profiles were shallower than 100 db, geopotential anomaly was calculated using the extrapolation technique described by Reid and Mantyla (1976). At 44°N where water greater than 100 m exists inshore of Heceta Bank, the Reid and Mantyla extrapolation was applied on both flanks of the Bank, i.e. going eastward from offshore and westward from inshore. At 44.25°N where the water inshore of Heceta Bank does not reach 100 m, the Reid and Mantyla extrapolation was just continued shoreward. Although a deeper reference level is desirable (e.g., 500 or 1000 m), previous studies have demonstrated the utility of the 100-m reference level for capturing the effect of upwelling on the pycnocline and the accompanying strong equatorward jet (e.g., Barth et al., 2000a).

2.3. Shipboard current profiles

Velocity profiles along the ship track were obtained using a shipboard 153.6-kHz narrowband acoustic Doppler current profiler (ADCP).

Measurement ensembles were obtained every 2.5 min using a pulse length of 12 m and vertical bin size of 8 m. When water depth is less than about 450 m, bottom tracking is used to reference the ship-relative velocities to an earth-based reference frame. In deep water, differential GPS is used for computing ship velocity. The shallowest reliable data were from 17 m. Other details of the data collection and processing follow Barth et al. (2000a) and the complete data set can be found in Pierce (2002). The overall error in a 5-min-averaged absolute ADCP velocity is estimated to be $\pm 0.02\ m\,s^{-1}$ when bottom tracking is available and $\pm 0.04\ m\,s^{-1}$ otherwise.

For maps of ADCP velocities, each vector is a 5 km spatial average in the horizontal and 10 m in the vertical. For vertical sections, 5-min ADCP data are contoured using a Barnes objective analysis scheme with three iterations (e.g., Daley, 1991) where the horizontal (vertical) grid spacing is 1 km (8 m), and the successive smoothing length scales are 10 km (50 m), 5 km (25 m) and 2.5 km (12.5 m). The usual caveat about aliasing low-frequency velocity fields by inertial oscillations applies, but strong coherence between the ADCP velocities and the dynamic height field suggests that this aliasing is minimal.

Transports are estimated from ADCP profiles by integrating the measured velocities down to 100 or 200 m. Velocities above 17 m are estimated by extending the 17-m value to the surface, i.e. a "slab" model at 17 m and above. Note that this will result in an underestimation of the transports because the jets in this region are vertically sheared (because they are in thermal wind balance with cross-jet density gradients). The total southward transport across a section is calculated by the above procedure, but just using the southward velocities. The error in ADCP-based transport estimates using a $0.01\ m\,s^{-1}$ systematic error across an E–W section is $0.05(0.10) \times 10^6\ m^3\,s^{-1}$ for the 100(200)-m deep calculation.

In most of the GLOBEC NEP study region, tidal currents from individual tidal constituents (e.g., M2, K1) are expected to be about $0.05\ m\,s^{-1}$, smaller than the subtidal velocity features described here. Using an array of current meters extending across the Oregon continental slope and shelf, Torgrimson and Hickey (1979) reported M2 (K1) semi-major axis amplitudes of 0.02–0.06 ($0.02-0.04$) $m\,s^{-1}$. Using a data-assimilating model together with high-frequency coastal radar and acoustic Doppler profiler velocities, Erofeeva et al. (2003) find similar magnitudes for the M2 and K1 currents except in a region directly over Heceta Bank, where K1 velocities reach $0.10\ m\,s^{-1}$ through a resonance of the tide with a first-mode barotropic shelf wave. Although the tidal currents are small in most of the study region, shipboard ADCP velocities are presented after removing an estimate of the tidal motion using the Erofeeva et al. (2003) tidal model. After removing the barotropic tidal currents from the ADCP measurements, a baroclinic tidal signal may still be present. The baroclinic tide is challenging to estimate and highly variable in time and space, as it depends upon the density structure in the water column. Semi-diurnal (M2) baroclinic tidal currents at the surface off Oregon can be as large as $0.10\ m\,s^{-1}$ (Torgrimson and Hickey, 1979; Kurapov et al., 2003).

2.4. Surface drifters

A total of nine surface drifters were present in the study region during the Mesoscale 2 survey. The WOCE-standard, holey-sock drifters were drogued at 15 m and tracked via satellite (Niiler et al., 1995). At this latitude, fixes are obtained roughly 9–12 times/day. The drifters are designed such that they slip less than $0.01\ m\,s^{-1}$ in $10\ m\,s^{-1}$ wind speed (Niiler et al., 1995). Five surface drifters were released on 8 July 2000 from 10 (18.5) to 65 (120.4) n mile (km) offshore along the Newport Hydrographic (NH) line (44.65°N) during a GLOBEC NEP LTOP cruise (Huyer et al., 2002) (Fig. 2). These drifters remained in the study region during the Mesoscale 2 survey as did two drifters released on the offshore end of the NH line in April 2000. Two drifters were released on 29 July 2000 at 10 and 15 n mile offshore on the NH line at the start of the Mesoscale 2 survey. Drifter trajectories are calculated by fitting a cubic smoothing spline (Reinsch, 1967) to the raw fixes, which minimizes the overall curvature while not allowing the root-mean-square deviation between

the fitted and the actual locations to exceed 1 km. Drifter velocities are then obtained by differencing the splined fixes. The GLOBEC NEP drifter data set can be found at http://diana.coas.oregonstate.edu/drift.

3. Results

Wind stress during the late-spring, early-summer large-scale mesoscale survey (30 May to 3 June, 2000) was upwelling favorable (southward) and relatively strong, reaching $0.2\,N\,m^{-2}$ (Fig. 2a). The wind in 2000 became generally upwelling favorable, with a commensurate drop in sea level, starting around 20 March (Fig. 2b). This transition to spring and summer conditions was interrupted by a 20-day period of northward winds and high sea level during late April and early May. Starting around 18 May, winds returned to generally upwelling favorable and remained so for the remainder of the spring-summer season except for occasional northward wind events. The strongest northward wind stress of nearly $0.4\,N\,m^{-2}$ occurred during the latter portion of the Mesoscale 1 survey. This strong northward pulse took place after the 5-d large-scale map was completed and resulted in downwelling and northward currents near the coast (O'Malley et al., 2002). After this event, the winds were strong and consistently upwelling favorable, pumping energy into the equatorward upwelling jet. Winds during the early part of the late-summer, large-scale mesoscale survey (30 July–4 August, 2000) were upwelling favorable and remarkably similar to those during late May, early June. That the wind forcing was nearly identical during these two surveys allows us to examine the seasonal evolution of the hydrographic, velocity and chlorophyll distributions without the confounding factor of variable wind stress. In comparison with the previous 15 years, the majority of the equatorward forcing during 2000 started late (mid-June) and was, in total, below average for the entire upwelling season (Fig. 2b). Although cumulative wind forcing during the cruises was nearly identical during the large-scale maps (about $0.5\,N\,m^{-2}\,d$), observations during late-summer reflect cumulative seasonal forcing of an additional $2.5\,N\,m^{-2}\,d$.

3.1. Late-spring, early-summer

Consistent with upwelling favorable wind forcing, cold water is apparent all along the coast in a satellite sea-surface temperature (SST) image from 1 June 2000 (Fig. 3). Cold water ($<12\,^{\circ}C$) is restricted to within about 50 km of the coast during this early part of the spring-summer upwelling season.

A map of 5-m temperature sampled with SeaSoar during 30 May–3 June 2000, shows a narrow band of cold water adjacent to the coast (Fig. 4). The width of the upwelling zone is larger over the Heceta Bank region in the north and south of Cape Blanco near 42.25°N. The upwelled, cold water generally follows the 200-m isobath (i.e. the shelfbreak) from Newport to Cape Blanco. South of Cape Blanco the region of cold water extends offshore of the 200-m isobath, consistent with previous observations of the separation of the coastal upwelling front and jet from the coast in this region (Barth et al., 2000a). The cold-water region is also consistent with the position of a geopotential anomaly contour ($\Delta\Phi = 2.35\,m^2\,s^{-2}$; see below for details), which indicates the location of the equatorward upwelling jet. Warm, oceanic water penetrates onshore of the 200-m isobath on the southern flank of Heceta Bank (near 44°N). This is likely a result of the upwelling jet turning cyclonically back onshore at the downstream end of the Bank and the beginning of a "lee" eddy-type effect early in the upwelling season. High-salinity surface water is also found inshore of the 200-m isobath and associated with the position of the equatorward upwelling jet (Fig. 5). Low-salinity surface water is apparent all along the offshore edge of the upwelling zone, with values less than 32.5, indicative of Columbia River influence (Huyer, 1983). The low-salinity surface feature is strongest in the north off Heceta Bank and salinities often become higher again offshore (i.e. on lines 1–5, 7 and 8), consistent with a ribbon of fresher water extending southward from the Columbia River (Huyer, 1983). Low-salinity water is found over the southern flank of Heceta

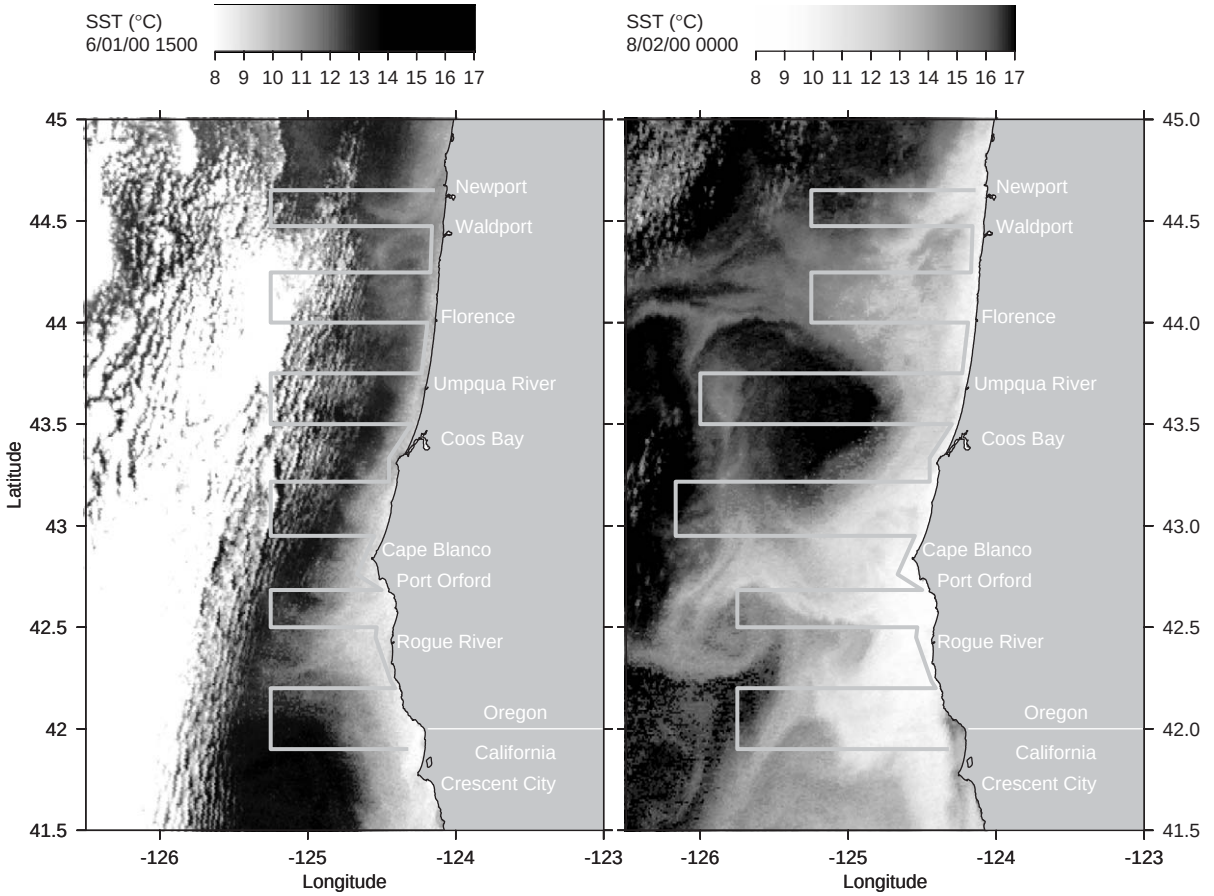

Fig. 3. Sea-surface temperature from satellite imagery during the early-summer Mesoscale 1 cruise (left) and late-summer Mesoscale 2 cruise (right). Ship survey grids are overlain in gray.

Bank, consistent with oceanic water penetrating farther shoreward in this location. Offshore of Crescent City (41.9°N) is a salty, warm surface feature, suggestive of water originating farther south and as found associated with anticyclonic eddies offshore in the California Current (Huyer et al., 1998). A vertical section of spiciness (Flament, 2002) (not shown) gives only a hint of high-spiciness water below 50 m in this feature. Although the spiciness signature of deep mesoscale offshore features this far north in the CCS at this time of year is expected to be weak, we did not have sufficient coverage in this survey to be definitive about the origin of this feature.

A map of geopotential anomaly at 5 m relative to 100 m shows that the equatorward upwelling jet follows, and is found inshore of, the 200-m isobath north of Cape Blanco (Fig. 6). Southward flow is proportional to the onshore E–W gradient in geopotential anomaly through the geostrophic relationship. The $\Delta\Phi = 2.35\,\mathrm{m^2\,s^{-2}}$ geopotential anomaly contour (dashed curve, Fig. 6) was chosen to indicate the location of the offshore edge of the core of the equatorward upwelling jet. The value $2.35\,\mathrm{m^2\,s^{-2}}$ was selected to highlight differences between late-spring–early-summer and late-summer (next section) when that contour delineates the offshore edge of the strongly meandering equatorward jet. The jet center passes inshore of the 200-m isobath over Heceta Bank (44–44.5°N), i.e. it is found inshore of the shelfbreak early in the upwelling season.

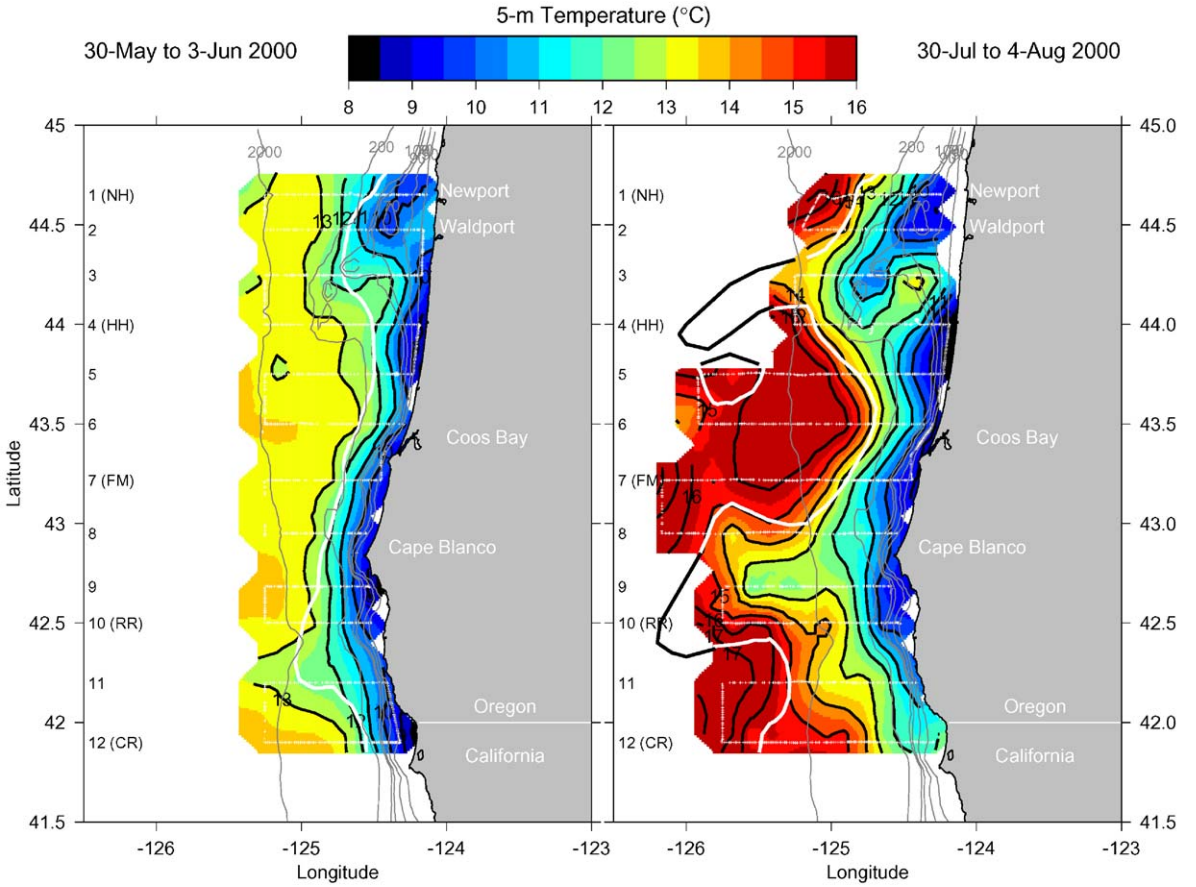

Fig. 4. Temperature at 5 m as measured by SeaSoar during the early-summer Mesoscale 1 cruise (left) and the late-summer Mesoscale 2 cruise (right). Measurements are from 1.25-km averaged bins along the survey track. The thick, white curve is the $\Delta\Phi = 2.35\ \mathrm{m^2\,s^{-2}}$ geopotential anomaly contour indicating the location of the equatorward jet. For the August survey, the $2.35\ \mathrm{m^2\,s^{-2}}$ contour outside the measurement region was drawn based on the location of the edge of the coastal upwelling region evident in a satellite SST image from 2 August 2000 (Fig. 3). The 50, 70, 90, 100, 200 and 2000-m isobaths are shown.

Downstream of Cape Blanco, the upwelling jet separates from the coast (lines 9–11) before turning back onshore to near the 200-m isobath off Crescent City. The salty offshore feature off Crescent City (41.9°N, 125°W) is compensated by warm temperatures so that the geopotential anomaly does not indicate the dynamic influence of this feature.

The equatorward upwelling jet reached speeds of $0.5\ \mathrm{m\,s^{-1}}$ based on tidally corrected currents at 25 m (Fig. 7). A significant onshore component is apparent on the southern flank of Heceta Bank (44°N, line 4). Note also the relatively weak velocities inshore of the Bank at 44.25° N (line 3). The core of the southward jet follows the $\Delta\Phi = 2.35\ \mathrm{m^2\,s^{-2}}$ geopotential anomaly contour except offshore on line 11. Further inspection of the velocity structure in this region leads us to believe that this feature is an inertial oscillation. The feature on line 11 is considerably weaker below 50 m than at shallower depths and the anticyclonic rotation of the velocity vectors going from offshore to onshore in time along line 11 is consistent with inertial motion. Although internal

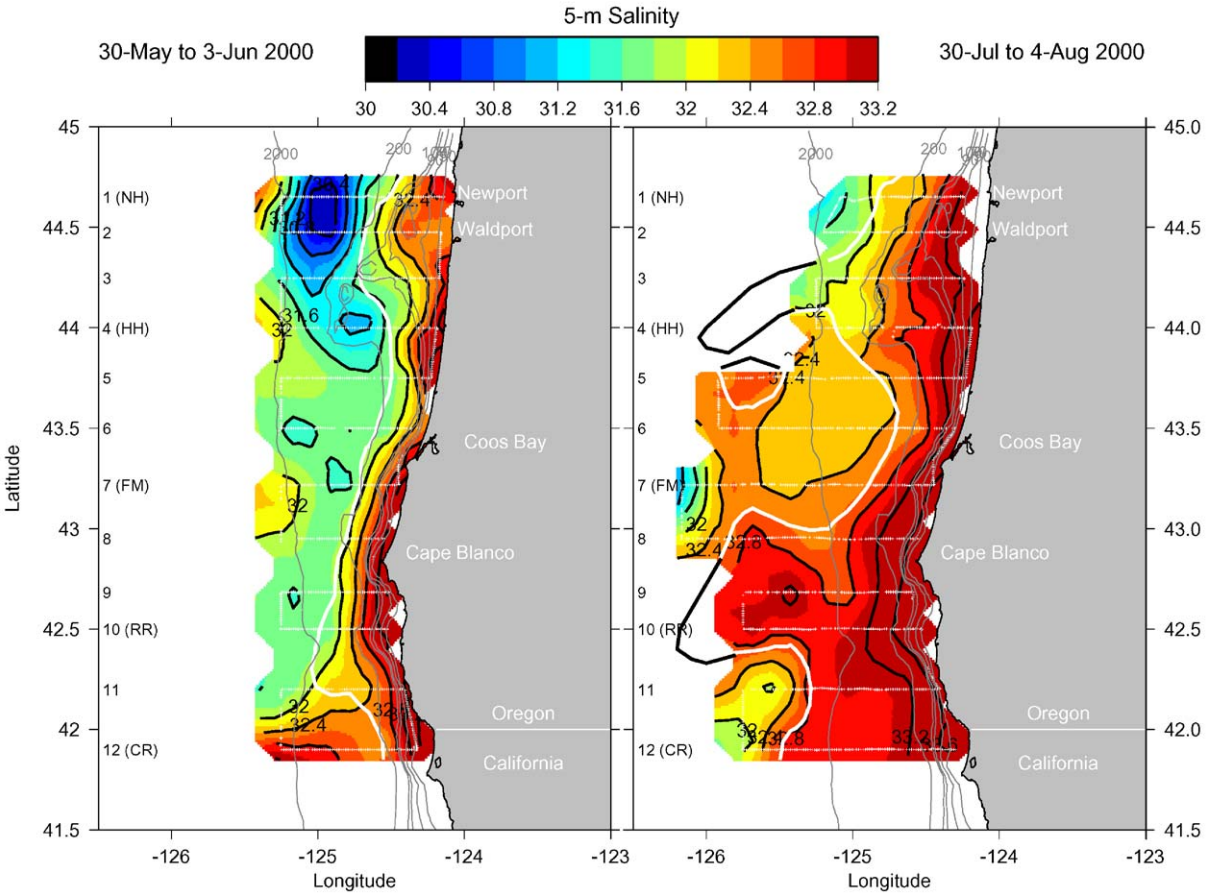

Fig. 5. Salinity at 5 m as measured by SeaSoar during the early-summer Mesoscale 1 cruise (left) and the late-summer Mesoscale 2 cruise (right). Measurements are from 1.25-km averaged bins along the survey track. The thick, white curve is the $\Delta\Phi = 2.35\ \mathrm{m^2\,s^{-2}}$ geopotential anomaly contour indicating the location of the equatorward jet. For the August survey, the $2.35\ \mathrm{m^2\,s^{-2}}$ contour outside the measurement region was drawn based on the location of the edge of the coastal upwelling region evident in a satellite SST image from 2 August 2000 (Fig. 3). The 50, 70, 90, 100, 200 and 2000-m isobaths are shown.

tides may also alias low-frequency velocity measurements, they are expected to be small ($<0.05\ \mathrm{m\,s^{-1}}$) this far offshore (1000 m depth), based on the results of Torgrimson and Hickey (1979). Filtering out the inertial motion, as the dynamic height calculation does, the equatorward jet turns back onshore south of line 11—note the consistent southeastward flow measured along a SW–NE line between lines 11 and 12—before continuing south in a concentrated jet off Crescent City. The mean (±1 SD) southward 0–200 m integrated transport in the equatorward upwelling jet is $1.4 \pm 0.3 \times 10^6\ \mathrm{m^3\,s^{-1}}$. This estimate uses shipboard ADCP data from sections where the jet crosses roughly orthogonally and that encompass the entire jet structure (lines 5–7 and 12).

Chlorophyll levels at 5-m in late-spring, early-summer were greater than $1\ \mathrm{mg\,m^{-3}}$ inshore of the 200-m isobath and were associated with the equatorward upwelling jet (Fig. 8). Highest values, reaching to around $4\ \mathrm{mg\,m^{-3}}$, were found in small patches over the Stonewall-Heceta Bank complex, near the coast off Coos Bay and inshore just to the south of Cape Blanco. Using data from the other lines south of Cape Blanco (lines 9–11) to plot chlorophyll values on the

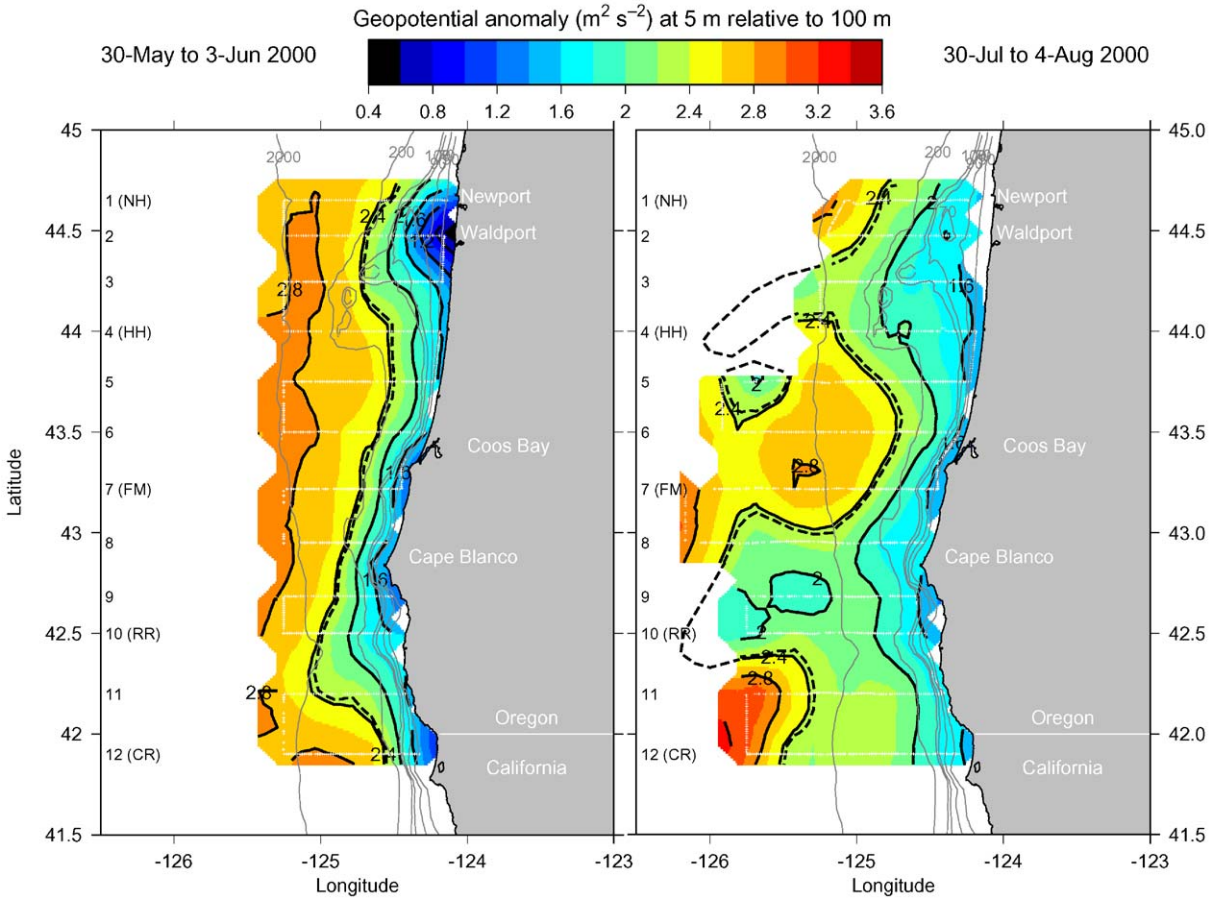

Fig. 6. Map of geopotential anomaly (dynamic height in meters multiplied by the acceleration of gravity) at 5 m relative to 100 m from SeaSoar surveys during 30 May to 3 June (left) and 30 July to 4 August (right) 2000. The dashed curve is the $\Delta\Phi = 2.35\ m^2\ s^{-2}$ contour. For the August survey, the $2.35\ m^2\ s^{-2}$ contour outside the measurement region was drawn based on the location of the edge of the coastal upwelling region evident in a satellite SST image from 2 August 2000 (Fig. 3). The 50, 70, 90, 100, 200 and 2000-m isobaths are shown.

$25.0\ kg\ m^{-3}$ σ_t isopycnal surface (not shown) reveals that an offshore subsurface chlorophyll maximum was present at 30 m depth flowing south in the separated upwelling jet, i.e. following the $\Delta\Phi = 2.35\ m^2\ s^{-2}$ geopotential anomaly contour. So chlorophyll is continuous along the coast associated with the upwelled isopycnals, but is concentrated close to the surface north of Cape Blanco and is found in a subsurface maximum south of Cape Blanco (see vertical sections of chlorophyll described in Section 3.3).

3.2. Late-summer

Late in the spring-summer upwelling season (August), there exists considerably more mesoscale variability in the satellite-derived SST (Fig. 3) than in early-summer. Cold-water surface features ($<14\ ^\circ C$) are found in excess of 150 km offshore, in particular off Heceta Bank (44°N) and Cape Blanco (42.8°N). Note that the gray scales for temperature differ in the two panels of Fig. 3 because they were chosen to highlight the location of the strongest SST fronts. For a comparison of

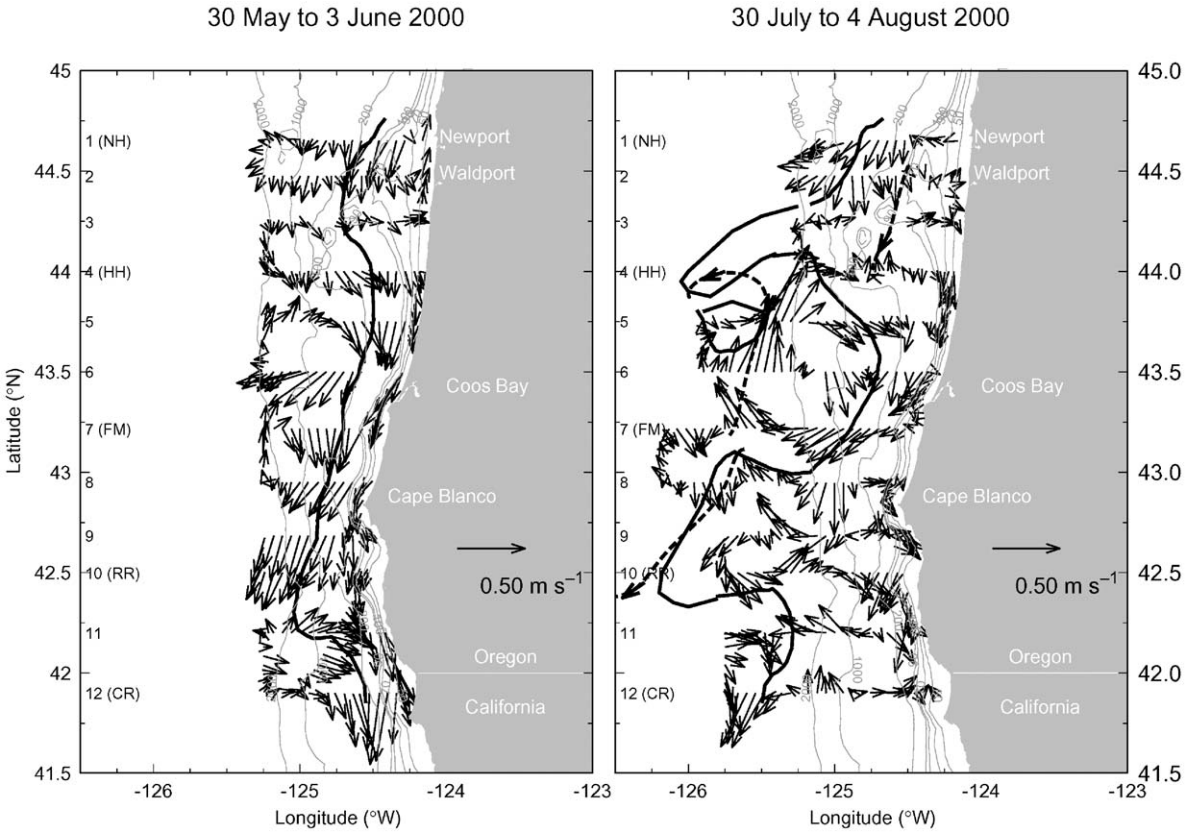

Fig. 7. Velocity at 25 m as measured by shipboard ADCP during the early-summer Mesoscale 1 cruise (left) and the late-summer Mesoscale 2 cruise (right). A scale arrow for velocity appears at right. The thick curve is the $\Delta\Phi = 2.35\ m^2\ s^{-2}$ geopotential anomaly contour indicating the location of the equatorward jet. Dashed curves on the Mesoscale 2 plot indicate the trajectories of three surface drifters during the time of that survey. The 50, 70, 90, 100, 200 and 2000-m isobaths are shown.

absolute SST, see Fig. 4. The SeaSoar/ADCP sampling grid was expanded farther offshore than during Mesoscale 1, but there was not sufficient time within a 5-d survey to extend all the lines far enough west to encompass all of the cold-water region. The 2 August 2000 SST (Fig. 3) image will be used to place the SeaSoar/ADCP measurements in a larger scale context.

The 5-m temperature field as measured by SeaSoar reveals a broad region of cold ($<13\,^{\circ}C$) upwelled water over the Heceta-Stonewall Bank complex (Fig. 4). While there is considerable seasonal warming in offshore waters ($\Delta \sim 3\,^{\circ}C$ since June), 5-m temperatures in the upwelled water are essentially the same as during Mesoscale 1, indicating the reduced influence of seasonal heating on subsurface waters prior to their upwelling. The temperature front bounding the cold upwelled region turns sharply westward around 44.5°N before returning into the sampling region near 44.0°N. By using the 2 August 2000 satellite SST image, the upwelling front can be connected through a cyclonic loop to the west as indicated by the thick black curve denoting the location of the $\Delta\Phi = 2.35\,m^2\,s^{-2}$ geopotential anomaly contour. The region of upwelled water near Coos Bay is similar to that found in May, i.e. a narrow band generally following the shelfbreak (200-m isobath). Upstream of Cape Blanco near 43°N, the upwelling front turns offshore and a continuous filament of relatively cold water is traceable northward along 126°W to the outer

edge of line 5. This represents a large anticyclonic meander in the upwelling front and jet (more details on the dynamic height and velocity below). The region of cold water ($<13\,^{\circ}C$) extends at least 90 km offshore of Cape Blanco. South of the Cape the upwelling front and jet turn back to the south with a split in the frontal gradient: $<15\,^{\circ}C$ near the shelfbreak and $>15.5\,^{\circ}C$ offshore around 125.75°W.

Another significant feature is the pool of warm water ($T>12.5\,^{\circ}C$) over the Heceta Bank complex (44.25°N, 124.4°W), inshore of the shallow offshore pinnacles of Heceta Bank. Results from Mesoscale 1 (Fig. 4, left panel) indicate that water in this region is influenced from offshore, e.g., as indicated by the position of the 12 °C isotherm. The warm pool is inshore of the southwestward tending coastal upwelling jet that is following the isobaths around the outside of the Heceta Bank complex and is transporting cold, upwelled water to the southwest (Oke et al., 2002a, b; Castelao and Barth, 2005). Local surface heating in the region of low flow velocity inshore of Heceta Bank (average July solar insolation value of $280\,W\,m^{-2}$; M. Levine, personal communication) would be more than enough (increase of 0.35 °C/day in a 20-m deep layer) to account for the observed warm temperatures. That the observed heating is less than this confirms that advection, both vertical and horizontal, plays a role in this region.

Salinity at 5 m shows high values coincident with cold upwelled water near the coast and extending offshore of Cape Blanco in a large anticyclonic meander. Surface salinities similar to those measured in the Columbia River plume during Mesoscale 1 ($S<32$) are only present far offshore on lines 1–3, 7–8 and 12 in early August, again confirming the greater offshore extent of the upwelling region later in the season. Higher surface salinities across the region are also consistent with reduced Columbia River runoff in late-summer. Surface salinity is consistently high across the Heceta Bank complex, confirming that the warm-water pool on the southern flank is upwelled water that has been influenced by local heating.

In early August, the coastal upwelling jet, as indicated by the $\Delta\Phi = 2.35\ m^2\,s^{-2}$ geopotential anomaly contour, is offshore of the shelfbreak and highly convoluted. The strong influence of the Heceta Bank complex and Cape Blanco are both evident. By using the 2 August 2000 satellite SST image, an estimate for the location of the $\Delta\Phi = 2.35\ m^2\,s^{-2}$ geopotential anomaly contour outside of the SeaSoar sampling grid off Heceta Bank (lines 3–4) and just south of Cape Blanco (lines 9–10) can be made. Off Heceta Bank the jet reaches far offshore (126°W, 160 km offshore) before turning back to the southwest to flow closer to the shelfbreak off Coos Bay. The jet turns strongly offshore just north of Cape Blanco, then continues to the northwest in this anticyclonic meander. Although the $\Delta\Phi = 2.35\ m^2\,s^{-2}$ contour does not connect with the high geopotential anomaly at 43.75°N, 125.75°W, drifter trajectories (Section 3.4) indicate that there is a continuous strong northward jet ($>0.4\,m\,s^{-1}$) continuing the anticyclonic meander. The jet then makes a 180° turn to the south near 43.8°N, 125.75°W) to continue southward on the outside of the cold, salty upwelled-water zone. Drifter trajectories also confirm this strong southward flow ($>0.4\,m\,s^{-1}$) along 125.9°W between 43.2 and 43.6°N. Lastly, on the inshore flank of the upwelling jet (e.g., the $\Delta\Phi = 2.0\ m^2\,s^{-2}$ geopotential anomaly contour), the flow more closely follows the shelfbreak, i.e. like the offshore edge of the core of the jet does earlier in the upwelling season.

The 25-m velocity field also shows the meandering nature of the coastal upwelling jet late in the upwelling season (Fig. 7). When interpreting this figure, it is important to remember that the vectors represent flow measured at the location of the tail of the vector. Inshore of the shelfbreak (200 m) the flow is generally equatorward except for just inshore of the shallow Heceta Bank pinnacles along 44.0°N. This north-northeast flow is consistent with a recirculation in the lee of the Bank and with the advection of offshore water onto the Bank (Fig. 4). As in late-spring–early-summer, velocities are weak inshore on the Bank at 44.25°N. Surface drifter trajectories during the time of the Mesoscale 2 survey (see Section 3.4) confirm the ADCP and dynamic height flow paths and illustrate conclusively the northward flow in the anticyclonic meander along 125.6°W and its 180° turn to the south near 44°N.

It is more difficult to estimate the equatorward transport in the meandering jet in August because few of the E–W sample lines cross the jet orthogonally. Using the southward flows on lines 2, 6 (inshore of 125.1°W) and 12 (offshore of 125.3°W), the mean (±1 SD) using 0–200 m shipboard ADCP velocities is $1.2 \pm 0.3 \times 10^6$ $m^3 s^{-1}$. This value is statistically indistinguishable from the late-spring–early-summer estimate indicating that the equatorward jet is carrying roughly the same amount of water.

In late-summer there was considerable alongshore variability in surface phytoplankton biomass, with values exceeding $20 mg m^{-3}$ over Heceta Bank and exceeding $5 mg m^{-3}$ well beyond the shelf break between lines 2–5 (Fig. 8). High concentrations also were found at several locations over the shelf near Cape Blanco and farther south. The separating coastal jet near Cape Blanco carries chlorophyll-rich surface water ($>5 mg m^{-3}$, e.g., 42.7°N, 125.5°W) far offshore. A ridge of relatively high chlorophyll along 125.8°W between 43.0°N and 43.75°N is found in the northward flowing segment of the anticyclonic meander.

3.3. Vertical structure

To illustrate the cross-shelf and depth structure of the hydrographic, velocity and chlorophyll fields, vertical sections from two latitudes are shown in Figs. 9 and 10. One section is from across Heceta Bank at 44.25°N (line 3) (Fig. 9) and the second from just south of Coos Bay at 43.22°N where the continental shelf is narrow (line 7, also known historically as the Five Mile line) (Fig. 10). In each figure, the left (right) panel shows results from early (late) in the upwelling season. The vertical sections are for lines occupied during the surveys shown in Figs. 4–8, except for the section at 44.25°N in August (Fig. 9, right panel) when instead a section from 5–6 August is used. This line along 44.25°N was completed less than two days after the line contributing to Figs. 4–8 and under very similar alongshore wind conditions (Fig. 2). We chose to show this line because it extends 20 km farther offshore and because the 4 August 44.25°N section unfortunately had a substantial amount of ADCP data missing right over Heceta Bank (Fig. 7, right panel). All the temperature sections show upwelling over the continental margin. Temperatures near the bottom inshore of the Heceta Bank pinnacle at 44.25°N are less than 7.5 °C, with considerably more cold, upwelled water present on the shelf in August, consistent with accumulated upwelling through the summer. Both temperature sections at 44.25°N show colder water at the surface above the shallow Bank (124.6–124.8°W in June; 124.5–124.7°W in August). In June, this is the cold water on the inshore side of the wind-driven equatorward upwelling jet which is flowing S–SW over the seaward side of the Heceta Bank complex (see Fig. 4). A warm surface feature inshore of Heceta Bank (124.4–124.6°W) is discernible in June and is distinct and up to 3 °C warmer than surrounding water in August.

The salinity sections across the Bank at 44.25°N also reflect spring-summer upwelling, with more saline water over the shelf in August. The Columbia River-influenced water ($S<32.5$) is found seaward of the upwelling front and reaches to 60(35) m depth offshore early(late) in the upwelling season. The lower salinities and greater depth influence of Columbia River water in June compared with August are again consistent with reduced river outflow through the summer. Note that in August, the warm surface feature inshore of Heceta Bank is not fresh, indicating the relative importance of local heating on this feature compared with advection from offshore.

Upper-ocean chlorophyll values are high over the Heceta Bank complex, in excess of $4 mg m^{-3}$ in early June and $20 mg m^{-3}$ in early August. Chlorophyll is high in both cold and warm surface waters, i.e. high values are not restricted to the warm pool inshore of the Bank in August. In June, there is a subsurface maximum of chlorophyll along the $25.0 kg m^{-3}$ density anomaly contour offshore of the Bank. This subsurface maximum along $25.0 kg m^{-3}$ is a fairly common feature in this region (see Fig. 10 and O'Malley et al., 2002).

The most striking aspect of the north–south velocity sections over the Heceta Bank complex (Fig. 9, bottom panels) is the presence of predominantly northward flow inshore of the Bank. The equatorward upwelling jet is located seaward of the shelfbreak as it flows around the

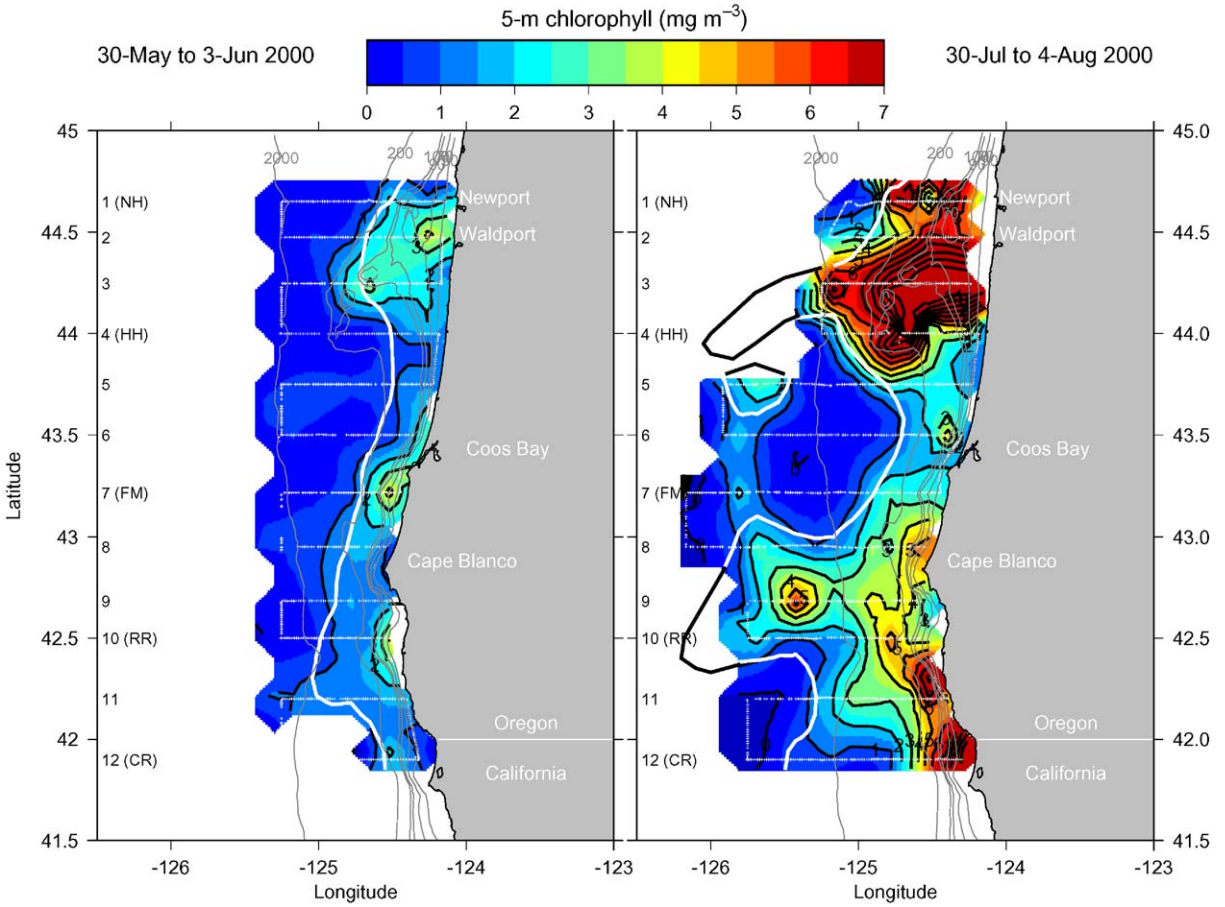

Fig. 8. Chlorophyll at 5 m as measured by SeaSoar during the early-summer Mesoscale 1 cruise (left) and the late-summer Mesoscale 2 cruise (right). Chlorophyll is derived from calibrated fluorescence. Values from offshore on line 12 during Mesoscale 1 were unavailable because the bio-optics system onboard SeaSoar was not properly receiving pumped water. Maximum values on Heceta Bank in August reach 20 mg m^{-3}. Measurements are from 1.25-km averaged bins along the survey track. The thick, white curve is the $\Delta\Phi = 2.35$ m^2 s^{-2} geopotential anomaly contour indicating the location of the equatorward jet. For the August survey, the 2.35 m^2 s^{-2} contour outside the measurement region was drawn based on the location of the edge of the coastal upwelling region evident in a satellite SST image from 2 August 2000 (Fig. 3). The 50, 70, 90, 100, 200 and 2000-m isobaths are shown.

Bank, and is found farther offshore in August consistent with the increased meandering of the jet later in the season. Inshore of Heceta Bank flow is northward, strongest at the bottom and reaching values of 0.2 m s^{-1}. In August, strong northward flow at depth over the shelfbreak offshore of the Bank (124.9°W) and extending down over the upper continental slope (not shown) is likely associated with the poleward undercurrent frequently present in this region (Pierce et al., 2000).

In contrast to the intraseasonal differences observed at 44.25°N over Heceta Bank, the hydrographic and velocity structure early and later in the upwelling season farther south at 43.22°N is relatively comparable inshore of 125.2°W (Fig. 10). Both sections show strong upwelling, the presence of Columbia River-influenced water offshore (stronger in June), and a classic horizontally and vertically sheared equatorward coastal upwelling jet carrying about 1.0 Sv between 0 and 100 m. The relative similarity of the

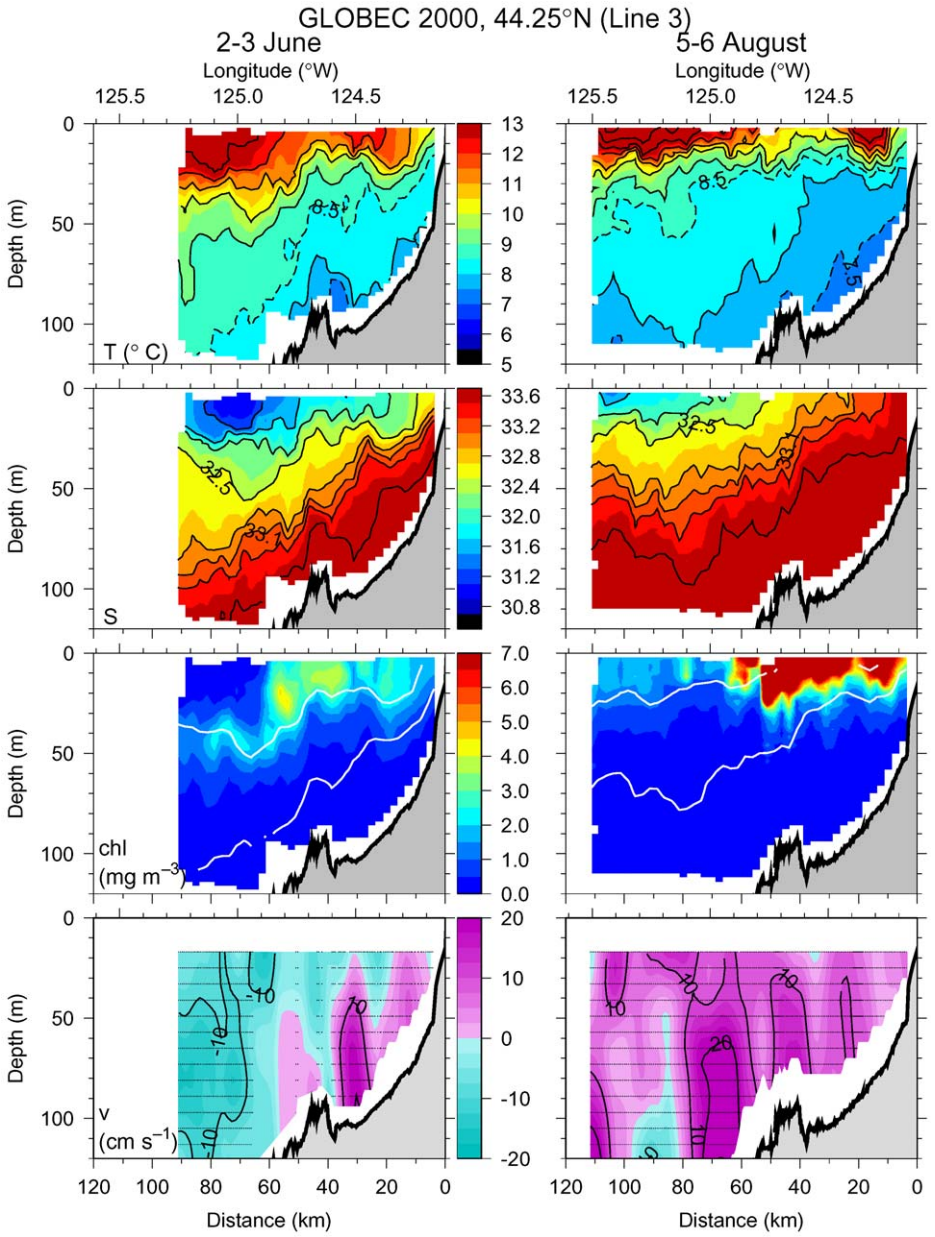

Fig. 9. Vertical sections along 44.25°N during 2–3 June (left) and 5–6 August (right) 2000. From top to bottom: temperature (°C), salinity, chlorophyll (mg m^{-3}) and north–south velocity (cm s^{-1}). White curves on the chlorophyll are the 25.0 and 26.0 kg m^{-3} density anomaly contours. Maximum chlorophyll values near the surface and inshore during August reach 24 mg m^{-3}.

fields through the season is likely a result of the importance of local wind driving over a relatively straight portion of narrow continental shelf. It also suggests that the influence of Heceta Bank does not reach south to this latitude.

Chlorophyll is high closest to the surface in the upwelled waters adjacent to the coast in both June and August at 43.22°N (Fig. 10), reaching values in June (>4 mg m^{-3}) comparable to those found farther north over Heceta Bank (Fig. 9). However,

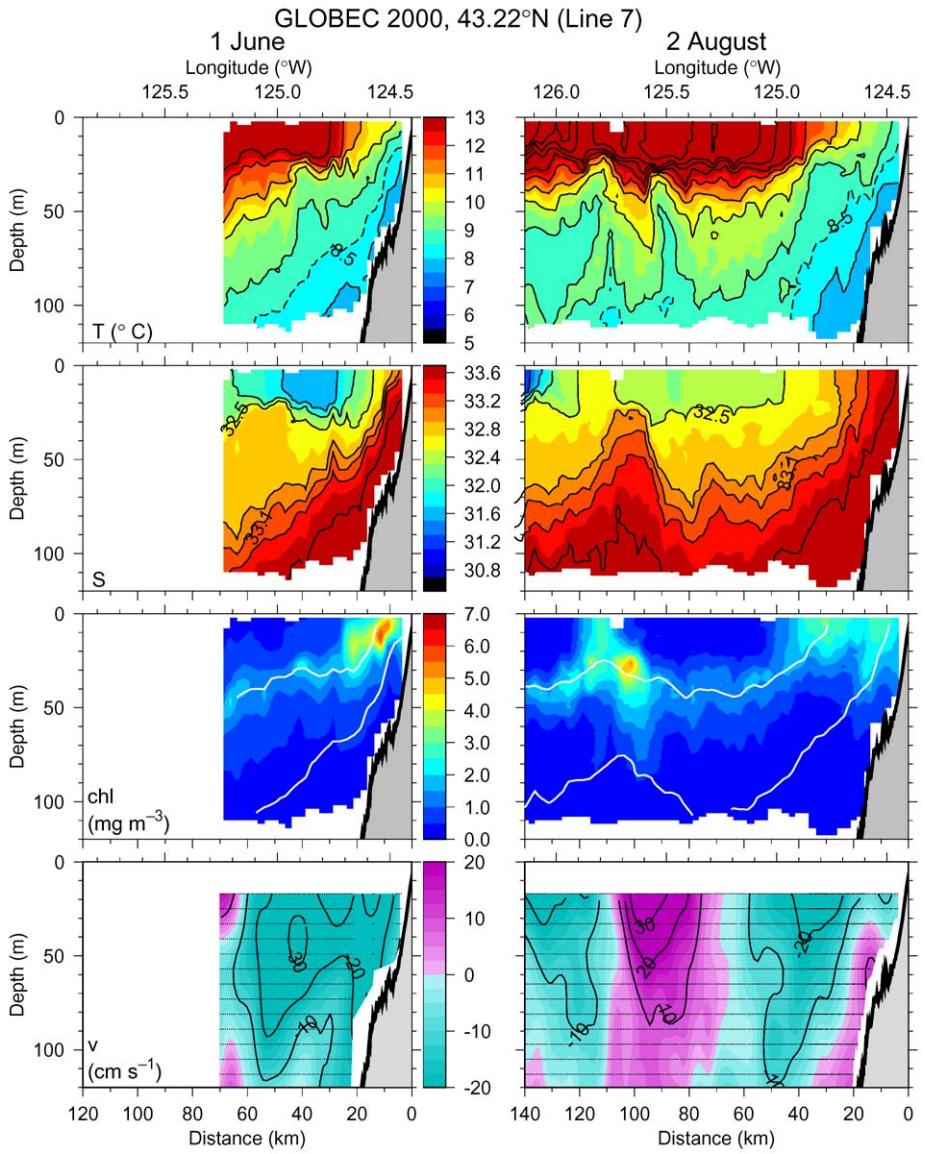

Fig. 10. As in Fig. 9, but along 43.22°N during 1 June (left) and 2 August (right) 2000.

in August, nearshore surface chlorophyll values are relatively low at this latitude, especially in comparison with the large values over Heceta Bank. Both sections of chlorophyll show subsurface maxima extending seaward along the 25.0 kg m^{-3} density anomaly contour.

The most obvious difference between the June and August sections at 43.22°N is the considerable mesoscale structure offshore of 125.2°W. The isotherms and isohalines reach their deepest depth at 125.3–125.4°W, resulting in a local maximum of dynamic height (Fig. 6). The isolines then turn upward farther offshore to form a ridge along 125.6–125.7°W. This ridge is the cold, saline upwelled water that has moved over 100 km offshore in the anticyclonic meander of the coastal upwelling jet. Consistent with the sloping isolines, northward velocity reaching 0.4 m s^{-1} is detected

in this region. Note that this northward flow has similar vertical shear to the equatorward jet farther inshore, reinforcing the interpretation that it is a separated coastal upwelling jet rather than a deep, anticyclonic eddy, which typically extend far deeper into the water column (Huyer et al., 1998). The isolines return to depth at the seaward end of the August section and are again accompanied by southward flow.

The separated coastal upwelling jet has drawn high chlorophyll water off the shelf to over 100 km from the shelfbreak. The maximum values in this chlorophyll feature are found near 30 m depth and are in excess of $5\,mg\,m^{-3}$. These values are higher than those found in surface waters adjacent to the coast at the same latitude, suggesting an origin near the coast closer to Cape Blanco along the path of the separated jet and then subsequent transport offshore (see Fig. 8). The fields in this region are clearly three-dimensional.

3.4. Surface trajectories

Trajectories of surface drifters spanning the time of the late-summer mesoscale survey reveal much about the circulation in this region (Fig. 11). They provide quasi-Lagrangian flow pathways because, while they follow the surface currents with only a small amount of slip due to windage on the low-profile surface buoy, they cannot follow water parcels that move vertically. All four drifters released within 15 nm (27.8 km) of the coast on the NH line (44.6°N), i.e. inshore of the 90-m isobath, on 8 and 29 July move S–SW at around $0.2\,m\,s^{-1}$ in the equatorward upwelling jet. The four drifters turn onshore at the southern end of the Bank and slow down considerably (speeds $<0.05\,m\,s^{-1}$). A low-velocity (speed $<0.10\,m\,s^{-1}$) region inshore of Heceta Bank is clearly evident in Fig. 11, consistent with shipboard ADCP velocities in this area (Fig. 7). Implications for the biological community in this region are discussed in Section 4. Prior to 11 August, three of these drifters re-enter the equatorward upwelling jet over the shelf south of Heceta Bank. The two drifters released on 8 July accelerate up to $0.5\,m\,s^{-1}$ in the jet. The drifter released at 15 nm offshore on 29 July enters the equatorward jet south of the Bank approximately three weeks after the drifters released on 8 July, hence its slower velocity in the jet. The drifter released at 10 nm offshore on 29 July does not enter the jet until after 11 August (not shown) where it then moves offshore in the separated jet near 43.25°N. The three drifters released on 8 July offshore of 25 nm at 44.6°N move to the W–SW consistent with offshore Ekman transport. The two closest to shore pick up speed (to $0.3–0.4\,m\,s^{-1}$) on the offshore extension of the meandering jet well offshore of Heceta Bank (44.0–44.5°N, offshore of 125.5°W). Elsewhere offshore the flow is generally $0.1\,m\,s^{-1}$ and less.

After separating from the coast just north of Cape Blanco, the two drifters diverge near 43°N, 125.5°W, where there is a valley in the dynamic height field (Fig. 6). One drifter decelerates and moves farther westward to join the strong (up to $0.5\,m\,s^{-1}$) southwestward flow of the meandering equatorward jet. It is eventually ejected from the jet at the cyclonic terminus of the upwelling filament and executes one cyclonic revolution before 11 August. The other drifter continues northward in the separated jet along 125.6°N at velocities up to $0.5\,m\,s^{-1}$. This velocity is consistent with the vertically sheared northward jet apparent in the vertical section of ADCP velocities at 43.22°N measured on 2 August (Fig. 10). At about 43.7°N, this drifter decelerates and moves westward, crossing the dynamic height valley to join the strong (up to $0.48\,m\,s^{-1}$) southward flowing equatorward jet along 125.9°W. Because of the narrow valley in dynamic height, it does not take much to move the drifters from one side of the valley to the other. This could be accomplished by strong Ekman transport, for example. In fact, this crossing of the dynamic height valley near 125.8°W happens three times (two described above) in the drifter tracks displayed in Fig. 11. The drifter crosses back into the northward jet near 43.2°N, transits rapidly northward again before exiting the meandering jet and being entrained in the onshore return flow (near 43.9°N) of the jet deflected around Heceta Bank. Finally, the drifter is entrained in the southward flow of the coastal upwelling jet near 124.8°N (c.f. the southwestward jet along 124.8°W in Fig. 10).

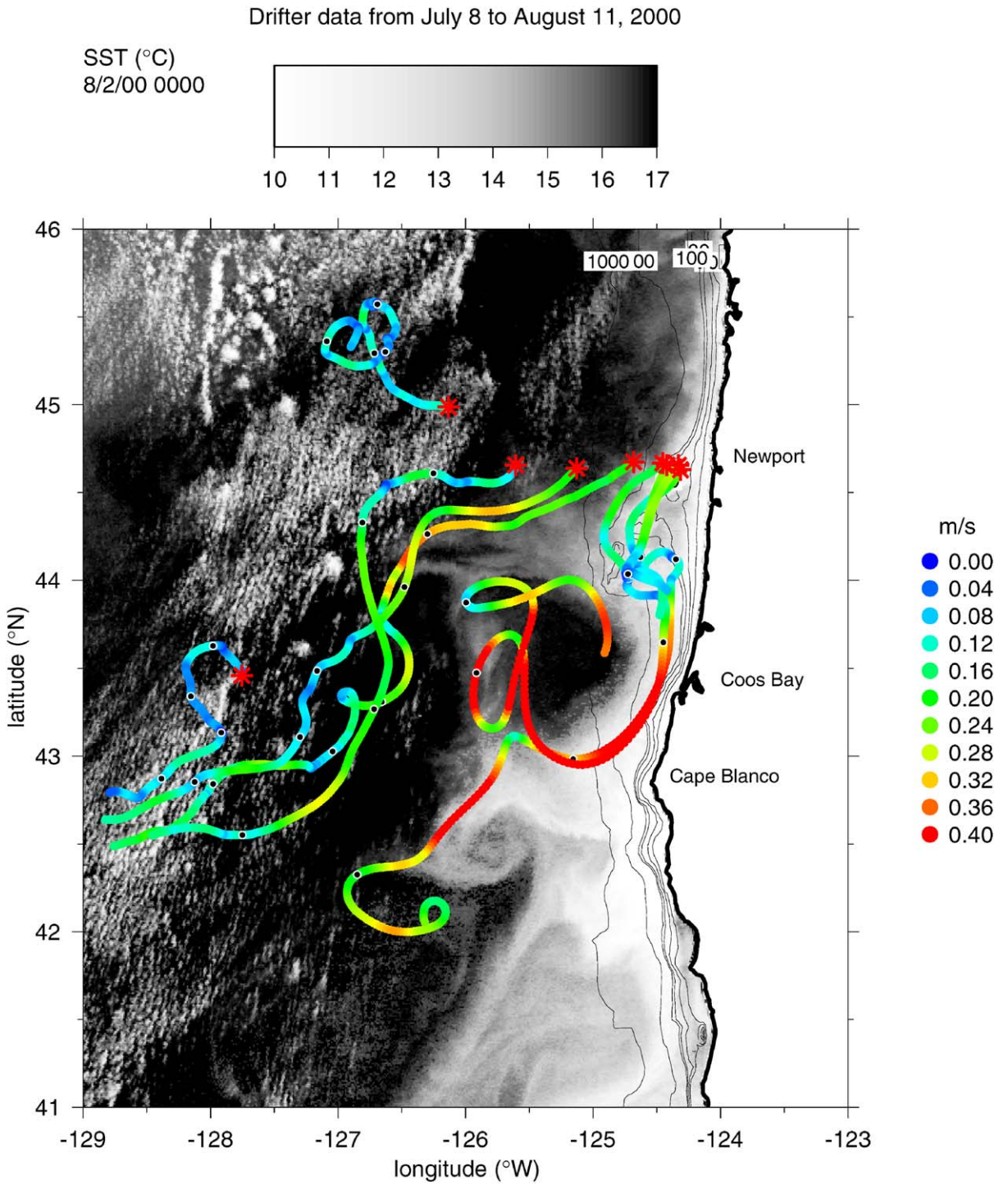

Fig. 11. Drifter trajectories from 8 July to 11 August, 2000, overlain on a satellite SST image from 2 August 2000. The trajectories start from the drifter's release location (red asterisks) off Newport except for northernmost and westernmost drifters that were released in April 2000, but remained in the study region. The trajectories are color-coded by drifter speed and black bullets along the tracks are at weekly intervals. The 50, 70, 90, 100, 200 and 1000-m isobaths are shown.

4. Discussion

One major result of this study is the observation of significant evolution of the hydrographic, velocity and chlorophyll distributions from early (May/June) to late (July/August) in the upwelling season in a region of flow–topography interaction. This evolution is a direct result of the input of energy from the wind into the kinetic and potential energy of the equatorward upwelling jet. This jet subsequently interacts with alongshore variations in topography (Heceta Bank, Cape Blanco) to create finite-amplitude meanders in the alongshore flow. In addition, the equatorward upwelling jet and front are known to undergo baroclinic instability once away from the stabilizing effect of the sloping continental margin topography (Barth, 1994; Haidvogel et al., 1991), contributing to the transfer of energy from the mean flow to the meander and eddy fields.

The mesoscale meanders of the equatorward upwelling jet associated with Heceta Bank and Cape Blanco apparent in the late-summer (August) survey develop as the spring-summer upwelling season progresses. The offshore diversion of the jet around Heceta Bank begins to occur early in the upwelling season (Figs. 3–7). In May, the core of the equatorward upwelling jet ($\Delta\Phi = 2.35\ m^2\,s^{-2}$ geopotential anomaly contour) is found flowing over the outer part of the Heceta Bank complex (Figs. 6 and 9). In other years, the core of the upwelling jet on the southern end of the Bank complex (44.25°N) is found along 124.6°W just inside of the Heceta Bank pinnacles as reported by Castelao and Barth (2005) for spring 2001. By early August, the jet flows around the outside of the Heceta Bank (Figs. 6 and 9) and the flow–topography is strong enough to drive flow significantly offshore before the jet turns back cyclonically toward the coast. There is interannual variability in the amount of the diversion of the flow around the Heceta Bank complex, with the amount of offshore motion in 2000 being greater than that observed in summer 2001 (Castelao and Barth, 2005).

The strong offshore meander just north of Cape Blanco first appears in satellite SST imagery around 20 June 2000 (not shown). The formation of the meander is likely due to intensified jet–topography interaction during the strong, sustained upwelling favorable wind event that started on 15 June and lasted until 3 July (Fig. 2). Surface drifters released on 8 July follow the pattern of the meandering equatorward jet measured in early August, in situ demonstration that the mesoscale structure existed at least since early July (Fig. 11). The strong meander off Cape Blanco is apparent in satellite imagery through early September. An image from 6 September (not shown) reveals a distinct westward meander evolved from the July–August pattern, but now starting at the coast around 42.75°N, south of Cape Blanco. Finding the root of the meander farther south is consistent with the fact that meanders due to baroclinic instability are known to propagate in the direction of the mean flow (southward in this case) (Barth, 1994). In summary, the strong mesoscale meandering associated with Cape Blanco observed in late-summer 2000 was present for up to 2.5 months.

The separation of the coastal upwelling jet near Cape Blanco is similar to the flow–topography interaction in summer 1995 described by Barth et al. (2000a). In August 2000, the jet separated slightly north of where it separated in August 1995. In 2000, the separation and subsequent anticyclonic meandering resulted in the flow turning due north about 100 km offshore before it turned back to flow equatorward. In contrast, in August 1995 the separated jet did not turn westward or northward, but only flowed southwestward south of Cape Blanco. That is, the subsequent anticyclonic meandering was substantially greater in 2000 than in 1995.

Although previous studies used slightly different definitions of equatorward transport in the coastal upwelling jet in this region, it is instructive to compare them with the present estimates. Barth et al. (2000a) reported transports from geostrophic velocities integrated from 0 to 200 m and estimated that $0.93 \times 10^6\ m^3\,s^{-1}$ was moving equatorward across 43°N during August 1995, indistinguishable from values estimated here for August 2000. Castelao and Barth (2005) report equatorward transport by integrating southward ADCP velocities down to 200-m for extensive observations

over Heceta Bank and just to the south (43.75°N) during 2001. Their values to the north and over Heceta Bank (44.0–45.25°N) are $0.68 \pm 0.20(0.43 \pm 0.20) \times 10^6\,m^3\,s^{-1}$ for early (late) summer, while the transport across 43.75°N (line 5) just south of the Bank was $1.38 \pm 0.37(1.25 \pm 0.56) \times 10^6\,m^3\,s^{-1}$ for early (late) summer. The values reported here for spring and summer 2000 are indistinguishable from the 2001 transports across 43.75°N (i.e. south of Heceta Bank). To compare with Castelao and Barth's (2005) estimates to the north and over Heceta Bank, southward transports for lines 1–4 in early-summer (no estimate was computed for late-summer because the E–W lines do not cross the jet orthogonally) yield $1.0 \pm 0.2 \times 10^6\,m^3\,s^{-1}$, larger but statistically indistinguishable from those for spring 2001.

The northward flow inshore of Heceta Bank (Figs. 9 and 10) is consistent with a "lee" effect as the equatorward upwelling jet flows around the Bank complex. Northward flow here can arise from the flow turning cyclonically back toward the coast on the southern part of the Bank complex. Note that the geostrophically adjusted flow in this region has a significant alongshore pressure (geopotential anomaly) gradient (Fig. 6). Changes to the geostrophic balance in this region, e.g., time-dependent wind forcing, may lead to northward, pressure-driven flow as described by Oke et al. (2002b). Northward pressure-driven flows on the shelf are often bottom intensified as the barotropic pressure gradient uniformly opposes the baroclinically sheared wind-driven southward flow (Oke et al., 2002b). Bottom intensification of the northward flow is apparent in Fig. 9.

The fact that low velocities are present inshore of Heceta Bank because the high-velocity coastal upwelling jet flows around the outer edge of the Bank complex (Figs. 7, 9 and 11) has profound implications for the biological response in this region. We note that low velocities inshore of Heceta Bank also are found in land-based coastal radar estimates of surface velocity (Oke et al., 2002a) and in Eulerian averages of surface drifters computed over six years of surface drifter data in this region (Barth and Erofeev, 2003). The low velocities inshore over Heceta Bank result in slower offshore advection of growing phytoplankton, and less dilution of that growing biomass by recently upwelled water that contains low concentrations of phytoplankton. This contrasts sharply with those areas north and south of Heceta Bank that have greater transport and associated upwelling velocities. That this is likely is corroborated by the warm surface water in this region during August (Fig. 4), a result of solar heating of the slowly moving upper-ocean. Nutrients are high over Heceta Bank (R. Letelier, personal communication), consistent with high salinity deep water upwelled there (Fig. 5). Thus retention and growth likely are responsible for the large phytoplankton biomass observed over the Heceta Bank complex (Fig. 8). In fact, in summer 2002 phytoplankton levels over Heceta Bank were $>30\,mg\,m^{-3}$ and the subsequent sinking and respiration of this organic matter were implicated in the appearance of hypoxic bottom water and die-offs of marine invertebrates (Grantham et al., 2004).

The low-flow region inshore of Heceta Bank may also serve to retain other organisms, for example, zooplankton as reported by Ressler et al. (2005) and Pierce et al. (2003). Additional analysis is needed to determine the balance between retention and loss in this area, but it is clear that phytoplankton biomass is high over the Bank and favors growth of zooplankton able to exploit this resource. Farther up the food chain, high abundances of marine mammals (Tynan et al., 2005), seabirds (Ainley et al., 2005) and juvenile salmon (Brodeur et al., 2004) are likely the result of high abundances of phyto and zooplankton over Heceta Bank.

5. Summary and conclusions

By using synoptic, high spatial-resolution surveys, the seasonal evolution of the hydrographic, velocity and chlorophyll fields in the northern California Current System have been detailed. These results should be useful for placing observations of other elements of the northern CCS food web (e.g., zooplankton, larval fish, birds and mammals) in a physical and primary productivity context. Upwelling favorable alongshore winds drive coastal upwelling and spin up an

equatorward jet. Early in the season, this jet is found inshore of the continental shelfbreak and follows the bottom topography. The region of cold, salty upwelled water is confined to over the shelf and modest levels of phytoplankton biomass are found associated with the upwelled water. Later in the summer upwelling season after continual energy input by the wind, the equatorward jet interacts strongly with alongshore topographic variations. The upwelling jet and front, and hence the width of the upwelling region, meander offshore off the Heceta Bank complex and near Cape Blanco. These mesoscale features carry coastal water and the material it contains over 100 km from shore. The features are long lived, lasting for around 2.5 months during the spring-summer 2000 upwelling season. This contrasts with the shorter time variability of velocity and hydrographic fields from the mid-shelf to shore (water depth <100 m) where the response to variability in the winds occurs on a 2–10 d time scale. In fact, currents close to shore can reverse completely in response to wind relaxation or reversal. During June 2000 there was a strong northward wind event reaching almost $0.4\,\mathrm{N\,m^{-2}}$ that resulted in substantial downwelling and northward currents, the details of which will be reported elsewhere.

Besides describing the formation and seasonal evolution of the meandering equatorward jet in this region, a major result is a description of the velocity, hydrographic and chlorophyll fields over the Heceta Bank complex. This major submarine bank diverts the alongshore coastal upwelling jet around its outer edge forming a region of reduced flow inshore and on the southern flank of the Bank. Low velocities in this region lead to increased importance of local surface heating, accumulation of phytoplankton biomass and potential retention of biological organisms.

Through comparison with other studies in this region during 1995 and 2001, some indication of the interannual variability of the mesoscale flow structure was described. The GLOBEC NEP program conducted similar mesoscale surveys to those described here in the upwelling season of 2002. A comparison of the hydrographic, velocity and chlorophyll distributions between 2000 and 2002 are left to a future paper.

A helpful comparative study of the seasonal evolution of upper-ocean circulation in this region is possible using satellite altimetry, land-based coastal radar and moored current meters. Finally, a more complete understanding of the physics (wind-driving, flow–topography interaction, intrinsic hydrodynamic instability) would benefit from detailed time-dependent, three-dimensional numerical modeling of this region. The features described here are robust and should be present in realistic models of this region. It is also hoped that ecosystem models, for example those based on nutrient-phytoplankton-zooplankton dynamics, would be helpful for investigating the order one differences in the biological response observed along the coast in this region.

Acknowledgements

We thank the officers and crew of the R.V. *Wecoma* for their tireless efforts in towing SeaSoar on our survey grids while coexisting amicably with the considerable fishing activity in this region. Oregon State University Marine Technicians, M. Willis, L. Fayler, T. Martin and D. Swensen were responsible for the highly successful SeaSoar operations. We thank R. O'Malley, A. Erofeev and C. Wingard for their help with collecting, processing and analyzing the voluminous data set presented here. This work was funded by National Science Foundation Grant OCE-0001035. Support for the surface drifters was provided by NSF Grant OCE-0000733 and additional support during the analysis phase of this project was provided by NSF Grant OCE-9907854. This is contribution number 471 of the US GLOBEC program jointly funded by the National Science Foundation and the National Oceanic and Atmospheric Administration.

References

Ainley, D.G., Spear, L.B., Tynan, C.T., Barth, J.A., Pierce, S.D., Ford, R.G., Cowles, T.J., 2005. Physical and biological variables affecting seabird distributions during the upwelling season of the northern California Current. Deep-Sea Research II, this issue [doi:10.1016/j.dsr2.2004.08.016].

Barth, J.A., 1994. Short-wavelength instabilities on coastal jets and fronts. Journal of Geophysical Research 99, 16095–16115.

Barth, J.A., Erofeev, A.Y., 2003. Surface drifter observations of the seasonal circulation in the northern California Current. Eos Transactions American Geophysical Union 84 (52) (Ocean Sci. Meet. Suppl., Abstract OC32-C11).

Barth, J.A., Pierce, S.D., Smith, R.L., 2000a. A separating coastal upwelling jet at Cape Blanco, Oregon and its connection to the California Current System. Deep-Sea Research II 47, 783–810.

Barth, J.A., Kosro, P.M., Pierce, S.D., 2000b. A submarine bank's influence on coastal circulation: Heceta Bank Oregon. Eos Transactions, Americal Geophysical Union, 81 (48) (Fall Meet. Suppl., F662).

Batchelder, H.P., Barth, J.A., Kosro, P.M., Strub, P.T., Brodeur, P.D., Peterson, W.T., Tynan, C.T., Ohlman, M.D., Botsford, L.W., Powell, T.M., Schwing, F.B., Ainley, D.G., Mackas, D.L., Hickey, B.M., Ramp, S.R., 2002. The GLOBEC Northeast Pacific California Current System program. Progress in Oceanography 15 (2), 36–47.

Brodeur, R.D., Fisher, J.P., Teel, D.J., Emmett, R.L., Casillas, E., Miller, T.W., 2004. Juvenile salmonid distribution, growth, condition, origin, and environmental and species associations in the Northern California Current. Fisheries Bulletin 102, 25–46.

Castelao, R.M., Barth, J.A., 2005. Coastal ocean response to summer upwelling favorable winds in a region of alongshore bottom topography variations off Oregon. Journal of Geophysical Research, submitted for publication.

Chelton, D.B., de Szoeke, R.A., Schlax, M.G., El Naggar, K., Siwertz, N., 1998. Geographical variability of the first-baroclinic Rossby radius of deformation. Journal of Physical Oceanography 28, 433–460.

Daley, R., 1991. Atmospheric Data Analysis. Cambridge Press, Cambridge, 457 pp.

Erofeeva, S.Y., Egbert, G.D., Kosro, P.M., 2003. Tidal currents on the central Oregon shelf models, data and assimilation. Journal of Geophysical Research 108 (C5), 3148 [doi:10.1029/2002JC001615].

Flament, P., 2002. A state variable for characterizing water masses and their diffusive stability: spiciness. Progress in Oceanography 54, 493–501.

Fogarty, M.J., Powell, T.M., 2002. An overview of the US GLOBEC program. Progress in Oceanography 15, 4–12.

Grantham, B.A., Chan, F., Nielsen, K.J., Fox, D.S., Barth, J.A., Huyer, A., Lubchenco, J., Menge, B.A., 2004. Upwelling-driven nearshore hypoxia signals ecosystem and oceanographic changes in the northeast Pacific. Nature 429, 749–754.

Haidvogel, D.B., Beckman, A., Hedstrom, K.S., 1991. Dynamical simulation of filament formation and evolution in the coastal transition zone. Journal of Geophysical Research 96, 15,017–15,040

Huyer, A., 1983. Coastal upwelling in the California Current System. Progress in Oceanography 12, 259–284.

Huyer, A., 1990. Shelf circulation. In: LeMehaute, B., Hanes, D.M. (Eds.), Ocean Engineering Science, The Sea, vol. 9, pt. A. Wiley, New York, pp. 423–466.

Huyer, A., Sobey, E.J.C., Smith, R.L., 1979. The spring transition in currents over the Oregon continental shelf. Journal of Geophysical Research 84, 6995–7011.

Huyer, A., Barth, J.A., Kosro, P.M., Shearman, R.K., Smith, R.L., 1998. Upper ocean water mass characteristics of the California Current, summer 1993. Deep-Sea Research II 45, 1411–1442.

Huyer, A., Smith, R.L., Fleischbein, J., 2002. The coastal ocean off Oregon and northern California during the 1997–8 El Niño. Progress in Oceanography 54, 311–341.

Kundu, P.K., Allen, J.S., 1976. Some three-dimensional characteristics of low-frequency current fluctuations near the Oregon coast. Journal of Physical Oceanography 6, 181–199.

Kurapov, A.L., Egbert, G.D., Allen, J.S., Miller, R.N., 2003. M_2 internal tide off Oregon: inferences from data assimilation. Journal of Physical Oceanography 33, 1733–1757.

Large, W.G., Pond, S., 1981. Open ocean momentum flux measurements in moderate-to-strong winds. Journal of Physical Oceanography 11, 324–336.

Lynn, R.J., Simpson, J.J., 1987. The California Current System: the seasonal variability of physical characteristics. Journal of Geophysical Research 95 (12), 12,947–12,966.

Niiler, P.P., Sybrandy, A.S., Bi, K., Poulain, P.M., Bitterman, D., 1995. Measurement of the water-following capability of holey-sock and TRISTAR drifters. Deep-Sea Research I 42, 1951–1964.

Oke, P.R., Allen, J.S., Miller, R.N., Egbert, G.D., Austin, J.A., Barth, J.A., Boyd, T.J., Kosro, P.M., Levine, M.D., 2002a. A modeling study of the three-dimensional continental shelf circulation off Oregon. Part I: Model-data comparisons. Journal of Physical Oceanography 32, 1360–1382.

Oke, P.R., Allen, J.S., Miller, R.N., Egbert, G.D., 2002b. A modeling study of the three-dimensional continental shelf circulation off Oregon. Part II: Dynamical analysis. Journal of Physical Oceanography 32, 1383–1403.

O'Malley, R., Barth, J.A., Cowles, T.J., Pierce, S.D., Wingard, C., 2002. SeaSoar CTD observations during the GLOBEC Northeast Pacific mesoscale surveys I, II, III and IV. WWW Page, http://damp.coas.oregonstate.edu/globec/nep/seasoar.

Pierce, S.D., 2002. Mesoscale and finescale mapping of physical and biological fields in the northern California Current System: Acoustic Doppler current profiler data. WWW Page, http://damp.coas.oregonstate.edu/globec/nep/adcp.

Pierce, S.D., Smith, R.L., Kosro, P.M., Barth, J.A., Wilson, C.D., 2000. Continuity of the poleward undercurrent along the eastern boundary of the mid-latitude north Pacific. Deep-Sea Research II 47, 811–829.

Pierce, S.D., Barth, J.A., Peterson, W.T., Cowles, T.J., 2003. Bioacoustic surveys in the northern California Current System: zooplankton retention mechanisms. Eos Transactions American Geophysical Union 84 (52) (Ocean Sci. Meet. Suppl., Abstract OS21-B23).

Pollard, R.T., 1986. Frontal surveys with a towed profiling conductivity/temperature/depth measurement package (SeaSoar). Nature 323, 433–435.

Reese, D.C., Miller, T.W., Brodeur, R.D., 2005. Community structure of near-surface zooplankton in the northern California Current in relation to oceanographic conditions. Deep-Sea Research II, this issue [doi:10.1016/j.dsr2.2004.09.027].

Reid, J.L., Mantyla, A.W., 1976. The effect of geostrophic flow upon coastal sea elevations in the northern North Pacific Ocean. Journal of Geophysical Research 81, 3100–3110.

Reinsch, C.H., 1967. Smoothing by spline functions. Numerische Mathematik 10, 177–183.

Ressler, P.H., Brodeur, R.D., Peterson, W.T., Pierce, S.D., Vance, P.M., Roestad, A.R., Barth, J.A., 2005. The spatial distribution of euphausiid aggregations in the northern California Current during August 2000. Deep-Sea Research II, this issue [doi:10.1016/j.dsr2.2004.09.032].

Strub, P.T., James, C., 2000. Altimeter-derived variability of surface velocities in the California Current System: 2. Seasonal circulation and eddy statistics. Deep-Sea Research Part II 47, 831–870.

Suchman, C.L., Brodeur, R.D., 2005. Abundance and distribution of large medusae in surface waters of the northern California Current. Deep-Sea Research II, this issue [doi:10.1016/j.dsr2.2004.09.017].

Sutor, M., Cowles, T.J., Peterson, W.T., Pierce, S.D., 2005. Acoustic observations of finescale zooplankton distributions in the Oregon upwelling region. Deep-Sea Research II, this issue [doi:10.1016/j.dsr2.2004.09.029].

Torgrimson, G.M., Hickey, B.M., 1979. Barotropic and baroclinic tides over the continental slope and shelf off Oregon. Journal of Physical Oceanography 9, 945–961.

Tynan, C.T., Ainley, D.G., Barth, J.A., Cowles, T.J., Pierce, S.D., Spear, L.B., 2005. Cetacean distributions relative to ocean processes in the northern California Current System. Deep-Sea Resarch II, this issue [doi:10.1016/j.dsr2.2004.09.024].

WET Labs, Inc., 1997, FlashPak User's Guide. Internal Report, Philomath, Oregon, 16 pp.

Zhou, M., Zhu, Y., 2002. Mesoscale zooplankton distribution and its correlation with physical and fluorescence fields in the California Current in 2000. Eos Transasctions American Geophysical Union 83 (4) (Ocean Sciences Meet. Suppl. Abstract OS21N-04).